ChemPubSoc Europe

DOI: 10.1002/slct.201901850

Chemistry SELECT Full Papers

Analytical Chemistry

Calcium-Induced Photoluminescence Quenching of Graphene Quantum Dots in Hard Water: A Quick Turn-Off Sensing Approach

Praveen Mishra[a] and Badekai Ramachandra Bhat*[b]

The photoluminescence of graphene quantum dots (GQD) is widely explored for sensory applications. Among various metal ions to be detected in aqueous bodies, Ca^{2+} ions are often neglected which is evident from the lack of literature. However, owing to booming industrialization, the available potable water is mostly crossing the prescribed hardness limits. Presented report summarize the synthesis of GQD via modified hydrothermal cutting of graphene oxide, which was further employed for sensing Ca^{2+} ions in hard water samples. The as synthesized GQD exhibited its characteristic blue photoluminescence on excitation with longwave UV ($\lambda \approx 365$ nm) which was suppressed on the introduction of Ca^{2+} ions. The GQD as photoluminescent probe determined the concentration of Ca^{2+} ion in water with an accuracy of 96.74% ± 3.26%. The LOD of the reported method was found to be 5 μM and it was sensitive towards Ca^{2+} ions in the presence of interfering ions such as Al^{3+}, Mg^{2+}, and K^{+} which are commonly found in hard water samples. Therefore, the determination of hardness of water w.r.t Ca^{2+} using GQD based PL turn off sensing is a quick, viable and economical method.

Introduction

Graphene Quantum Dots (GQD) are zero-dimensional graphene with a finite band gap. The quantum confinement effect associated with the quantum dot leads to the photoluminescence.[1] The reported size of GQDs is usually within the range of 3–20 nm.[2] These properties of GQD makes it widely used for a variety of purposes, including the production of photovoltaic devices,[3] organic light-emitting diodes,[4] fuel cells,[5] and drug delivery systems.[6] The ease of synthesis of GQDs is another attribute which makes them choicest probe for such applications.[7]

In recent years, GQD has found widespread applications as sensors.[8] The sensing ability of GQD ranges from metal ions to toxic anions, from biomolecules to oxidants, and from toxins to explosives. Different modes of sensing platform GQD are used for can be divided chiefly in electrochemical sensor, photoluminescent/fluorescent sensors, colorimetric sensors, and hybrid sensors. GQD have shown immense potential in electrochemical sensing of biomolecules, like DNA,[9] proteins,[10] amino acids,[11] uric acid,[12] glucose,[13] and even detection of the virus.[14] Therefore, GQD is the choicest material for biosensing applications.

Use of GQD as a fluorescent platform are reported with success for various metal ions[8] such as Al^{3+},[15] Fe^{3+},[16] Cu^{2+},[17] Cr^{6+},[18] Hg^{2+},[19] Ni^{2+},[17d] Mn^{2+},[17d] Co^{2+},[17d,e] Ce^{3+}.[20] The detection of these metal ions is of industrial significance. However, in domestic use, water sample does not contain these ions. Hence these probes may not be used in such cases. Ca^{2+} is the most commonly found ion in domestic water samples responsible for the hardness of water.

Calcium is one of the most commonly found element in the water and biological system. Calcium is an essential dietary supplement for the development of the human body. It is directly involved in the growth of bones and cartilages. Presence of calcium in water is a measure of the hardness of water, and consumption of hard water is shown cause various health hazard.[21] The irregularities in the calcium intake, more specifically in large intakes can reportedly lead to ailments like prostate cancer, cardiovascular disease, preeclampsia, kidney stone, and weight loss.

The methods of determining calcium reported in the literature are very few and sophisticated. Determination of calcium used chromophores or molecules which can give visual aid can be helpful for the process on the go. Biochromatic squaraine dye based foldamers were one such reported to selectively determine Ca^{2+} calorimetrically with success.[22] The reported molecule showed a 1:1 binding with Ca^{2+}. The optical signal is this mode of detection is observed when the bichromophore fold around the Ca ion which leads to the excitonic coupling between the two squaraine chromophores. Fluorescent molecules specifically designed for determining the cation are proven and efficient platform for the quantitative determination which may offer quick sensing approach.[23] Among the most popular known flurorescent probe for demining Ca^{2+}, an 8-coordinate tetracarboxylate chelating site with stilbene chromophores was employed by Grynkiewicz et. al.[24] Major limitations of these sensing platforms happen to be

[a] P. Mishra
Catalysis and Materials Laboratory, Department of Chemistry, National Institute of Technology Karnataka, Surathkal, Mangalore 575025, India
[b] Prof. B. R. Bhat
Catalysis and Materials Laboratory, Department of Chemistry, National Institute of Technology Karnataka, Surathkal, Mangalore 575025, India
E-mail: ram@nitk.edu.in

Supporting information for this article is available on the WWW under https://doi.org/10.1002/slct.201901850

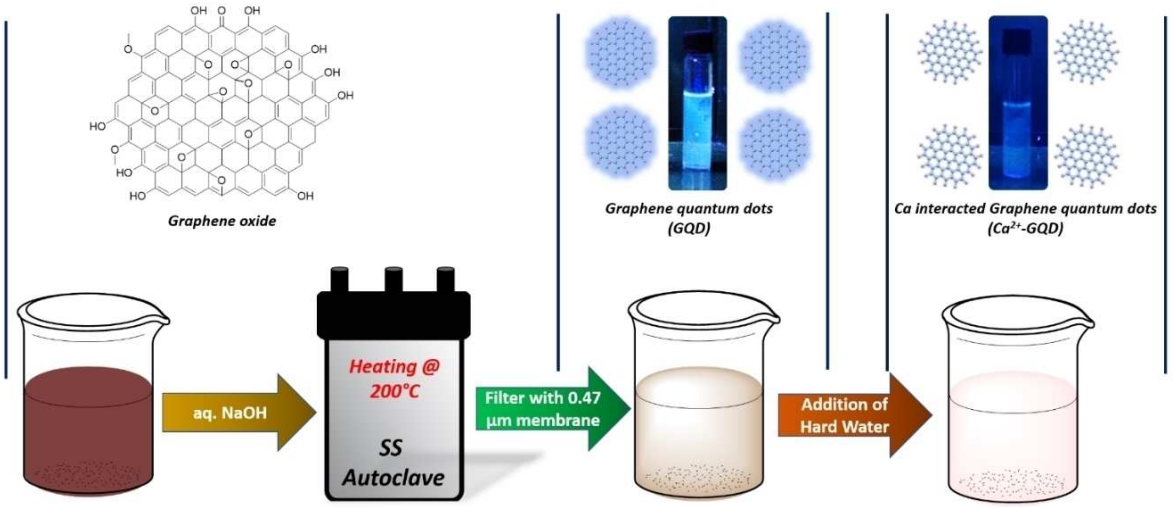

Scheme 1. A schematic of the synthesis of graphene quantum dots and its subsequent quenching of photoluminescence in hard water.

difficult synthesis methods. An interesting development based on the fluorescent probes was made by Suzuki et.al. by fabricating a fiber optics-based probe based on a natural carboxylic polyether antibiotic.[25] Other methods include state of the art techniques like wavelength dispersive X-ray fluorescence and laser-induced breakdown spectroscopy in the biological samples with success.[26] Ozbek et. al. determined the amount of calcium in rice varieties using induced plasma atomic emission spectroscopy.[27] These methods although able to estimate the content of Ca in trace amounts are not universally applicable. Due to very limited and available reports on the determination of Ca ions, there is a need to explore a much quick and economical way to determine calcium in the aqueous system. Here, we report a GQD based PL turn sensor for the determination of Ca^{2+} ions. Aim of the study is to develop a very fast qualitative tool for the detection of Ca^{2+} in aqueous and biological samples.

Results and Discussion

The schematic representation of the experimental procedure is given as Scheme 1. The details of the procedure followed are provided in the experimental section. To summarize the process, the highly photoluminescent GQD were obtained from the hydrothermal cutting of graphene oxide as reported elsewhere[28] with modifications. The PL quenching in GQD is a well-documented phenomenon for transition metals and lanthanides in literature.[16b,g, 17e, 20] Therefore, a similar approach was attempted to result in the quenching of deep blue photoluminescence by the introduction of Ca^{2+} ions. Calcium was selected as the primary analyte for this study due to it being the primary reason for the hardness of water. The subsequent quenching of the PL observed in GQD dispersion on the introduction of Ca^{2+} ions means they can be qualitatively determined. The observed effect further prompted an investigation for the quantitative determination of the Ca^{2+} ion in the hard water samples. As demonstrated in the Scheme 1, the workflow of the experiment involves the synthesis of GQD with deep blue PL by the hydrothermal cutting[28] of graphene oxide,[29] which was subsequently was arrested by the introduction of Ca^{2+} ions. Another takeaway from the scheme is the fact that there is a plausible scenario where Ca^{2+}, owing to its divalent nature interacts with two GQD resulting in the relaxation of the excitonic barrier which leads to the photoluminescence quenching which is a common occurrence in case of transition metals.[16b,17e] However, this phenomenon is not reported in the literature for the alkali and alkaline earth metals to the best of our knowledge. The primary reason for this may be the smaller size of these cations. However, among the common cations present in the hard water, Ca have shown to exhibit excellent PL quenching phenomenon in the GQD dispersion. We will discuss the results obtained which lead to the conclusion about the possible use of GQD for quantitatively determining the amount of Ca^{2+} in the hard water samples and the intrinsic limitation which this system presents.

Graphene oxide was used as the precursor synthesize GQD. The quality of the precursor plays an important role in the properties of the GQD obtained. The graphitic stacks present in the precursor may lead to improper fragmentation during the hydrothermal process. This as a result, means highly stacked fragments of GQD would be obtained which have poor PL. Therefore, graphene oxide was analyzed using x-ray diffraction to ascertain its physical characterization. The characteristic broad peak observed at a diffraction angle (2θ) of 10.2°. This peak corresponds to the (002) plane of graphene oxide[30] (Figure 1a). The observed peak was a significant departure from the highly intense and sharp peak at observed at 2θ of 26° for graphite (inset Figure 1a). Additionally, the complete absence of any peak at 26 or near about signifies that the highly pure graphene oxide was obtained. Additionally, there is a virtual absence of the graphitic stacking in the obtained graphene oxide which was a result of proper intercalation during the

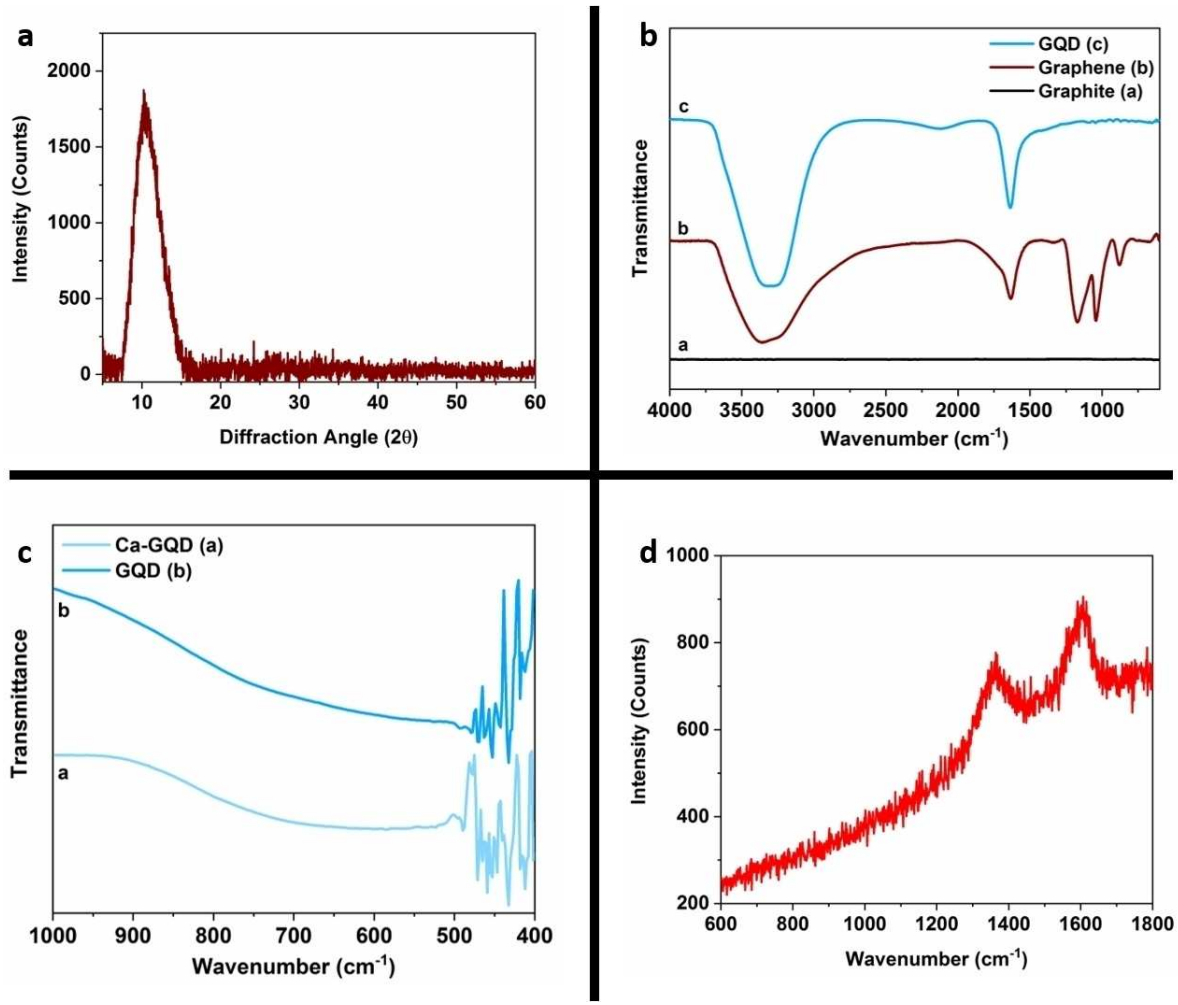

Figure 1. a) XRD spectrum of graphene oxide (Inset: XRD spectrum of graphite); b) FTIR spectra of graphite, graphene oxide and GQD; c) Finger print region of GQD and Ca-GQD; d) Raman spectra of GQD.

oxidation process. The oxidation of graphite also adds oxygen rich functional moieties in the graphene sheets which are the primary characteristic of graphene oxide. The purity of graphene oxide is also important as the formation of the GQD depends on the oxygen rich functional groups present in graphene oxide.[28] As discussed by pan et. al., the cleavage of the graphene oxide sheets takes place at the ethoxy groups present due to the high pressure and temperature of the hydrothermal process. The role of oxygen containing functional groups can be visualized by the FTIR analysis.

The FTIR spectra (Figure 1b) of graphite, graphene oxide, and GQD were recorded to exhibit the changes in the available functional groups in each of the stages. Graphite is a layered structure of sp^2 carbon arranged honeycomb lattice. The absence of any functional group means that there was no characteristic transmission peak observed. Therefore, the spectrum of graphite was observed as a straight line. Graphene oxide is a functionally rich carbon nanostructure with various oxygen bearing functional groups namely carboxylic (–COOH; –OH stretching 3300 cm^{-1} and –C=O stretching 1700 cm^{-1}), hydroxyl (–OH stretching 3500 cm^{-1}), carbonyl (–C=O stretching 1680 cm^{-1}), ether (–C–O–C– stretching 1250 cm^{-1}) and anhydride groups (–CO–O–OC– stretching, 1080 cm^{-1}) were observed at their respective wavenumber. GQD is formed when the ether and highly unstable anhydride groups are cleaved. The fragmentation of these groups leads to the formation of additional carbonyl (–C=O) and hydroxyl (–OH) groups in the GQD. Therefore, the characteristic peaks corresponding to the ether and anhydrides are absent in the FTIR spectrum of GQD. Hence, the FTIR results ascertain the formation of GQD. On the introduction of Ca^{2+} ion in the dispersion of GQD, the –COOH groups play an important role in binding to the calcium ions.[31] Ca^{2+} binds strongly to the carboxylic groups with bond strength stronger than certain heavy metals.[31a] The binding of Ca^{2+} ions with the carboxylic group of GQD was confirmed by comparing the fingerprint region FTIR of the GQD and Ca^{2+} interacted GQD (Ca-GQD) (Figure 1c). It clearly shows the presence of Ca–O bending vibrations at 415 cm^{-1},[32] which is absent in the spectrum of GQD. Therefore, it was concluded that the Ca^{2+} binds to the carboxylic group of GQD. It must be

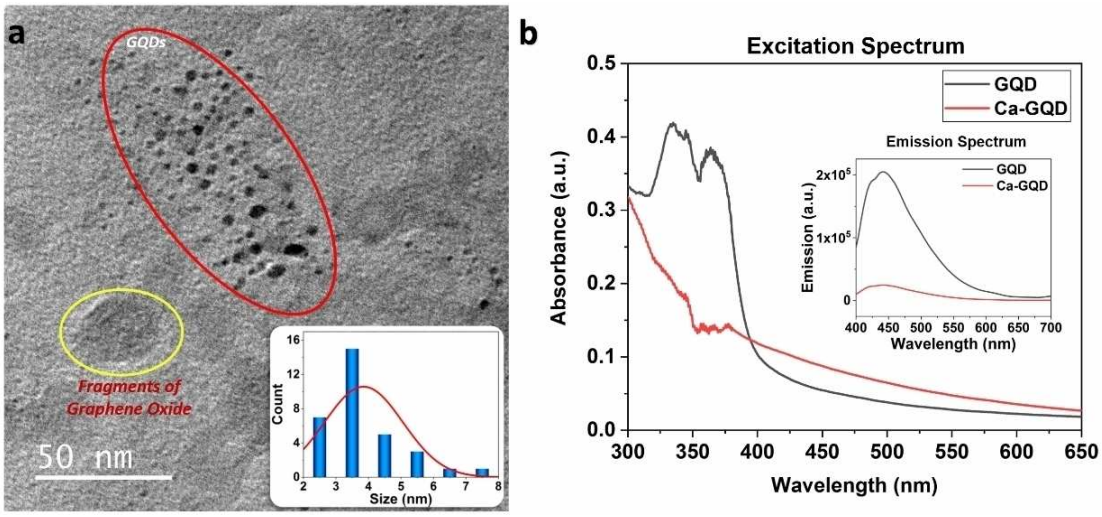

Figure 2. (a) Transmission electron micrograph of GQD and their size distribution (inset), (b) UV absorbance spectra of GQD and Ca-GQD

noted that unreacted carboxylic acid groups will exhibit themselves as their respective characterization peaks. Hence, the use of finger print region of the FTIR spectroscopy is essential to observe the Ca–O binding. The Raman spectra of GQD was observed with characteristic D band and G band at 1350 cm^{-1} and 1580 cm^{-1}, respectively commonly associated with graphene. The 1:1 ratio of the D and G band intensities signals towards the appreciable loss of graphitic layered structure. The ration of intensities also means that the synthesized GOQ are mostly bi-atomic layer or tri-atomic layer thick. This is the direct influence of the highly pure graphene oxide precursor used for the synthesis of GQD.

The transmission electron micrograph of the quantum dots reveals the visual cues about the size and the size distribution of GQD (Figure 2a). The average size of GQD was observed to be approximately 3.5 nm in diameter. The size distribution of the GQD was also very narrow, with 93% of GQD being within the size of 3 to 5 nm. The narrow size distribution is highly essential for observing sharp PL. This is because the size of GQD has a direct effect on the PL.[33] Hence, the as-synthesized GQD produced a deep blue luminescence. The UV-Vis absorbance spectra of GQD and Ca-GQD is presented as Figure 2b. GQD absorbs electromagnetic radiation within the range of 320–400 nm with two absorbance peaks at 340 nm and 375 nm. The addition of Ca^{2+} ion to the GQD significantly reduces the absorbance, which is the case in the UV-Vis spectrum of Ca-GQD. The interaction of Ca^{2+} ions with GQD make empty d-orbitals available for the electronic transition which reduces the energy required for the excitation of the electrons. Hence, we observe a rise in the absorption of electromagnetic irradiance from 400 nm to 650 nm, which is higher than the absorbance observed for GQD. The gradual availability of the lower energy required for the excitation of electron means that the absorbance of Ca-GQD is significantly reduced at 340 nm and 375 nm, respectively. This reduction in the absorbance is early signs of the eventual loss in PL in Ca-GQD. This is because the intensity of PL emission is also dependent on the absorbance in the UV-Vis region. The loss in absorbance and the relaxation of excitonic barrier cumulatively reduce the observed PL in the Ca-GQD. The absorbance at 375 nm results in the PL emission at 450 nm, which is corresponding to visible blue color (Inset Figure 2b).

The effect of Ca^{2+} on PL of GQD on a first glance seems similar to that mentioned for other metal ions[8] in the literature such as Al^{3+},[15] transition metals like Fe^{3+},[16] Cu^{2+},[17] Cr^{6+},[18] Hg^{2+},[19] Ni^{2+},[17d] Mn^{2+},[17d] and Co^{2+},[17d,e] and lanthanides like Ce^{3+}.[20] The study involving cerium (a lanthanide) as an analyte reports the direct suppression in the PL intensity of GQD due to the redox reaction between Ce^{3+} ion on the GQDs surface. This is possible as Ce benefits with having 2 stable oxidation states of +3 and +4 which is actively involved in the process of PL quenching. Other transition metal ions such as Fe usually require the modification in the GQD with groups like1-butyl-3-methylimidazolium (BMIM)[16b] or heteroatom like nitrogen.[16g] In such cases, the reason behind the apparent suppression of the PL intensity is deemed to be the relaxation in excitonic barrier which is caused by the metal ions. However, the GQD itself is not selective towards the heavier transition metal ions therefore the need of modification arises. GQD, however was observed to be selective in binding with Ca^{2+} ion (discussed later) with appreciable PL quenching. The mode of PL quenching here is not based on the redox behavior, as was the case with Ce^{3+} ions due to a single stable oxidation state of Ca. The reason for the apparent PL quenching was the relaxation of the excitonic barrier as is the case with the modified GQD binding to transition metals, however, with the exception that the binding in present case is with the as-synthesized GQD without the need of any modification. Furthermore, the loss of absorption as near the excitation wavelength as evident in the Figure 2a also results in the reduced PI observed. Hence, the loss of PL intensity is a cumulative result of the lower absorbance of excitation wave and the relaxation of excitonic

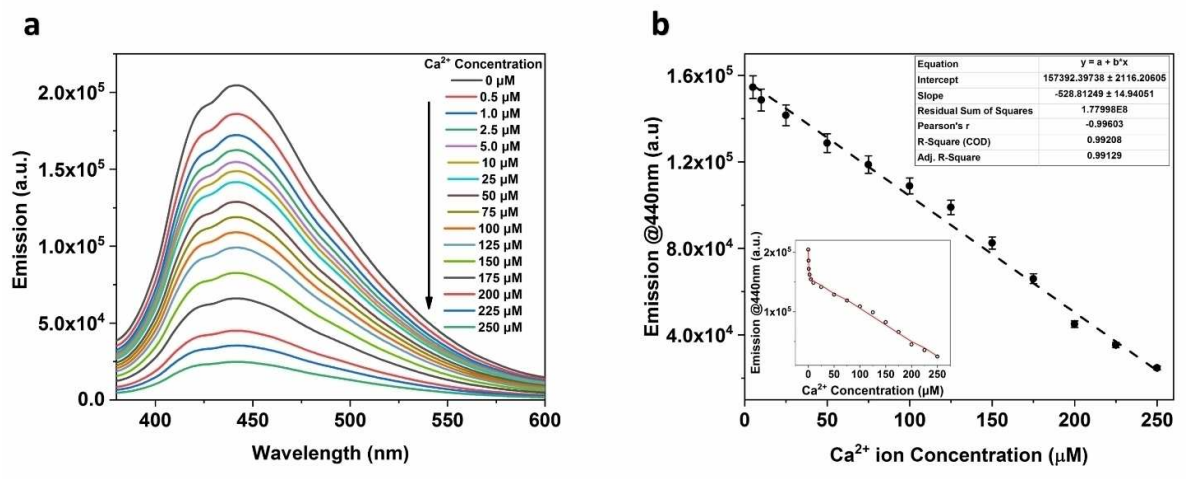

Figure 3. (a) The variation of photoluminescence of GQD in various solutions containing 0 μM to 250 μM Ca^{2+} ions respectively, under 365 nm irradiation, (b) linear relation of the photoluminescence quenching of GQD at different concentrations of Ca^{2+}.

Table 1. The photoluminescence measurements and the calculated strength of the test sample of Ca^{2+} ions with varying concentration.

S. No.	Actual Conc. (μM)	Expected PL (a.u)	Observed PL (a.u)	Determined Conc. (μM)	PL emission Accuracy (%)	Conc. Of Ca^{2+} Accuracy (%)
1	80	115152	112240	85	97.5 ± 2.5	93.7 ± 6.3
2	120	94032	96540	115	97.3 ± 2.7	95.8 ± 4.2
3	160	72912	74787	156	97.4 ± 2.6	97.5 ± 2.5
4	200	51792	49266	204	95.1 ± 4.9	98 ± 2.0
5	240	30672	32062	237	95.5 ± 4.5	98.7 ± 1.3
Average Accuracy in measurement (%)					96.56 ± 3.44	96.74 ± 3.26

barrier due to the charge transfer capability of Ca^{2+} ions. Therefore, the reported mode of detection of Ca^{2+} ion is quite different from the similarly available literature.

As is evident with the discussion so far, photoluminescence is a significant property for GQD. They exhibit a typical blue luminescence when excited with an incident beam of 375 nm. This PL emission is further utilized to quantitatively determine the amount of Ca^{2+} ion in an aqueous media. The loss of absorbance in the UV-Vis spectra and earlier known phenomenon on excitonic relaxation in the metal interacted GQD, it is understood that the mode of detection will be based on the PL quenching which in simpler terms can be called as a "Turn-off" sensor. Figure 3a shows the observed quenching in the PL intensities of GQD at various concentration of Ca^{2+} in the solution. As is evident from the graph, the extent of the PL quenching is directly related to the concentration of Ca^{2+} in the solution. The quenching of the PL is a result of the combined effect of the lower absorbance of the excitation energy, and the relaxation of excitonic boundaries in the Ca^{2+} interacted GQD which facilitates charge transfer among the quantum dots bound to the Ca^{2+} ion.

As observed form the figure, the extent of PL quenching is gradual with the increase in the concentration of Ca^{2+} ions in the solution. The relation between the PL quenching and the concentration of Ca^{2+} ions is presented in Figure 3b. The PL quenching was found to be linear to the concentration of the Ca^{2+} ions with a coefficient of regression of 0.99129. The linearity between the observed PL and concentration was valid till 5 μM Ca^{2+} ions in water (Inset Figure 3b)). Therefore, it was concluded that the limit of detection (LOD) of Ca^{2+} ions is 5 μM. The variable size and availability of the functionality on the edges of the GQD mean that the interaction between the Ca^{2+} ions and the GQD are not in a fixed stoichiometric ratio.

The performance of the GQD as a sensing platform was evaluated using some water samples of known concentrations (80, 120, 160, 200, and 240 μM). The expected PL values based on the calibration curve plotted in Figure 3b for the water samples are compared with the observed PL in Figure 4a. Both expected and observed PL values were in close agreement, and the calculated concentrations of the test samples are given in Table 1. The observed intensity of photoluminescence was in good agreement with the expected intensity of photoluminescence as determined by the equation of the linear fit of the curve in Fig 3b. The average accuracy was 96.56 ± 3.44% for the measurement of photoluminescence intensity. Similarly, the concentrations of Ca^{2+} ions determined in the test samples were having an average accuracy of 96.74 ± 3.26%. These results signify the potential of the reported method to determine the amount of Ca^{2+} ion in aqueous solutions.

The common cations found in the potable water samples apart from Ca^{2+} are Mg^{2+} and Al^{3+}. The GQD were highly sensitive towards Ca^{2+} ions as compared to the Mg^{2+} and Al^{3+} ion (Figure 4b). This is possibly due to the larger size of Ca^{2+} ions as compared to the Mg^{2+} and Al^{3+} ions, which facilitate

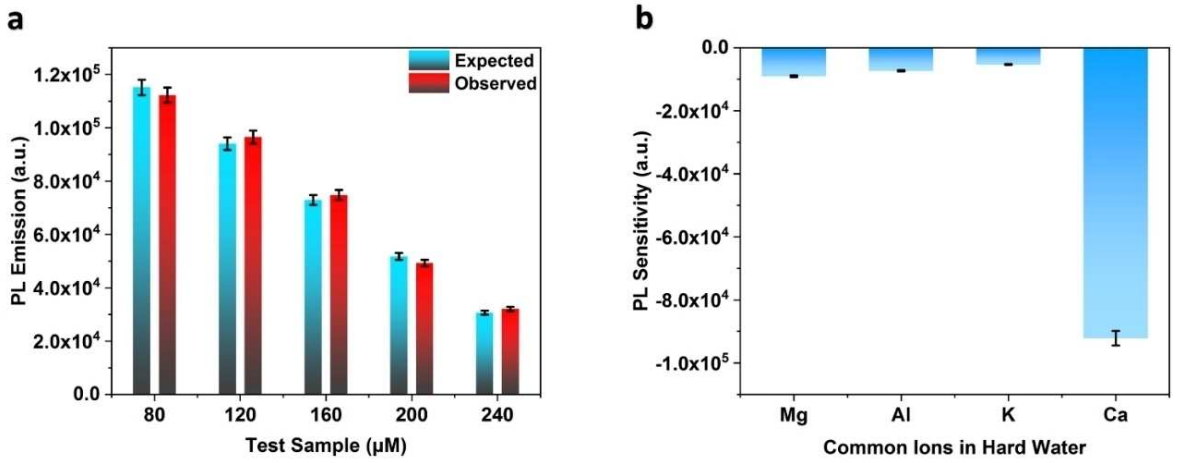

Figure 4. a) The expected and observed photoluminescence of various test samples of Ca^{2+} ion as detected by GQD under 375 nm irradiation; b) the selectivity of photoluminescence quenching of GQD towards Ca^{2+} in the presence of other common cations found in hard water.

higher PL quenching. However, the presence of transition metals may interfere in proper detection of Ca^{2+} ions due to the competing PL quenching of GQD.

Table 2 compares the results obtained for the use of GQD as a sensory platform for the Ca^{2+} ions with the other techniques used for the determination of the said cation in literature. As it is evident, the accuracy of the presented mode of determination is comparable to that of highly sophisticated techniques like WDXRF, LIBS, and Microwave induced plasma AES within the linear range of 5 μM – 250 μM. The method is more suitable that various others, owing to ease of preparation of GQD and its availability in humblest of the setups.

Table 2. Comparison of the reported sensing method for Ca2 + ions with other methods

S.No.	Mode of Determination	Detection Range	Limit of Detection	Accuracy	Reference
1	Bichromophoric Squaraine Foldamer	NA	NA	NA	[22]
2	Fluorescent photoinduced electron transfer cation sensors	NA	NA	NA	[23]
3	Fluorescent Indicators	Only Qualitative	Few mM	NA	[24]
4	Fibre Optic Sensor	10-7 M - 10–1 M	10-7 M	NA	[25]
5	Wavelength dispersive X-ray fluorescence (WDXRF) and	NA	0.1% (w/w)	99.9%	[26]
6	Laser-induced breakdown spectroscopy (LIBS)	NA	0.1% (w/w)	99.9%	[26]
7	Microwave induced plasma atomic emission spectrometry	13 μg.L-1 - 10 g. L − 1	13 μg.L-1	93.9%	[27]
8	GQD	5 μM – 250 μM	5 μM	96.74%	This Work

Conclusions

In conclusion, the hydrothermal cutting of GO sheets was used to synthesize GQD, which lead to a reduction in the size of the GO sheet. This size reduction is responsible for the excitonic entrapment within the GQD structure, which is the cause of observed photoluminescence. The observed interaction between Ca^{2+} and GQD core was due to the bond formation between Ca^{2+} ion and carboxylic groups on the edges of GQD. This interaction leads to the quenching of PL in GQD. The reason for the quenching was the apparent lowering in the absorption of UV irradiation of 375 nm and also because of the long range conjugation around Ca^{2+} ions which relax excitonic barrier. This PL quenching also referred to "turn-off" mechanism of sensing, was employed to determine the concentration of Ca^{2+} ions in the aqueous media. The reported method was able to determine the strength of Ca^{2+} ions with an accuracy of 96.74 ± 3.26% and limit of detection being 5 μM. Therefore, the reported method may be used as a quick and economic alternative to determine the amount of Ca^{2+} ion in potable water samples.

Supporting Information Summary

The detailed experimental section is provided in the Supporting Information.

Acknowledgements

Author, Mr. Praveen Mishra would like to acknowledge National Institute of Technology Karnataka for extending the research fellowship.

Conflict of Interest

The authors declare no conflict of interest.

Keywords: Calcium ion · graphene quantum dots · hard water · photoluminescence · sensing

[1] R. Liu, D. Wu, X. Feng, K. Müllen, *J. Am. Chem. Soc.* **2011**, *133*, 15221–15223.
[2] F. Chen, W. Gao, X. Qiu, H. Zhang, L. Liu, P. Liao, W. Fu, Y. Luo, *Frontiers in Laboratory Medicine* **2017**, *1*, 192–199.
[3] I. P. Hamilton, B. Li, X. Yan, L.-s. Li, *Nano Lett.* **2011**, *11*, 1524–1529.
[4] L. Tang, R. Ji, X. Cao, J. Lin, H. Jiang, X. Li, K. S. Teng, C. M. Luk, S. Zeng, J. Hao, S. P. Lau, *ACS Nano* **2012**, *6*, 5102–5110.
[5] Y. Li, Y. Zhao, H. Cheng, Y. Hu, G. Shi, L. Dai, L. Qu, *J. Am. Chem. Soc.* **2012**, *134*, 15–18.
[6] X. Wang, X. Sun, J. Lao, H. He, T. Cheng, M. Wang, S. Wang, F. Huang, *Colloids Surf., B* **2014**, *122*, 638–644.
[7] M. Bacon, S. J. Bradley, T. Nann, *Part. Part. Syst. Charact.* **2014**, *31*, 415–428.
[8] S. Benítez-Martínez, M. Valcárcel, *TrAC, Trends Anal. Chem.* **2015**, *72*, 93–113.
[9] J. Zhao, G. Chen, L. Zhu, G. Li, *Electrochem. Commun.* **2011**, *13*, 31–33.
[10] L. Li, W. Li, C. Ma, H. Yang, S. Ge, J. Yu, *Sens. Actuators, B* **2014**, *202*, 314–322.
[11] Q. Zhang, C. Song, T. Zhao, H.-W. Fu, H.-Z. Wang, Y.-J. Wang, D.-M. Kong, *Biosens. Bioelectron.* **2015**, *65*, 204–210.
[12] M. Mazloum-Ardakani, R. Aghaei, M. Abdollahi-Alibeik, A. Moaddeli, *J. Electroanal. Chem.* **2015**, *738*, 113–122.
[13] H. Razmi, R. Mohammad-Rezaei, *Biosens. Bioelectron.* **2013**, *41*, 498–504.
[14] X. Wang, L. Chen, X. Su, S. Ai, *Biosens. Bioelectron.* **2013**, *47*, 171–177.
[15] Z. Fan, Y. Li, X. Li, L. Fan, S. Zhou, D. Fang, S. Yang, *Carbon* **2014**, *70*, 149–156.
[16] a) H. Xu, S. Zhou, L. Xiao, H. Wang, S. Li, Q. Yuan, *J. Mater. Chem. C* **2015**, *3*, 291–297; b) A. Ananthanarayanan, X. Wang, P. Routh, B. Sana, S. Lim, D.-H. Kim, K.-H. Lim, J. Li, P. Chen, *Adv. Funct. Mater.* **2014**, *24*, 3021–3026; c) L. Zhou, J. Geng, B. Liu, *Part. Part. Syst. Charact.* **2013**, *30*, 1086–1092; d) S. Li, Y. Li, J. Cao, J. Zhu, L. Fan, X. Li, *Anal. Chem.* **2014**, *86*, 10201–10207; e) L. Li, L. Li, C. Wang, K. Liu, R. Zhu, H. Qiang, Y. Lin, *Microchim. Acta* **2015**, *182*, 763–770; f) T. Van Tam, N. B. Trung, H. R. Kim, J. S. Chung, W. M. Choi, *Sens. Actuators, B* **2014**, *202*, 568–573; g) J. Ju, W. Chen, *Biosens. Bioelectron.* **2014**, *58*, 219–225.
[17] a) H. Sun, N. Gao, L. Wu, J. Ren, W. Wei, X. Qu, *Chem. - Eur. J.* **2013**, *19*, 13362–13368; b) X. Liu, W. Gao, X. Zhou, Y. Ma, *J. Mater. Res.* **2014**, *29*, 1401–1407; c) F. Wang, Z. Gu, W. Lei, W. Wang, X. Xia, Q. Hao, *Sens. Actuators, B* **2014**, *190*, 516–522; d) H. Huang, L. Liao, X. Xu, M. Zou, F. Liu, N. Li, *Talanta* **2013**, *117*, 152–157; e) P. Mishra, B. R. Bhat, *Macromol. Symp.* **2017**, *376*, 1600200.
[18] F. Cai, X. Liu, S. Liu, H. Liu, Y. Huang, *RSC Adv.* **2014**, *4*, 52016–52022.
[19] a) B. Wang, S. Zhuo, L. Chen, Y. Zhang, *Spectrochim. Acta, Part A* **2014**, *131*, 384–387; b) H. Chakraborti, S. Sinha, S. Ghosh, S. K. Pal, *Mater. Lett.* **2013**, *97*, 78–80.
[20] F. Salehnia, F. Faridbod, A. S. Dezfuli, M. R. Ganjali, P. Norouzi, *J. Fluoresc.* **2017**, *27*, 331–338.
[21] C. Jayasumana, S. Gunatilake, P. Senanayake, *Int. J. Environ. Res. Public Health* **2014**, *11*.
[22] E. Arunkumar, A. Ajayaghosh, J. Daub, *J. Am. Chem. Soc.* **2005**, *127*, 3156–3164.
[23] B. Valeur, I. Leray, *Coord. Chem. Rev.* **2000**, *205*, 3–40.
[24] G. Grynkiewicz, M. Poenie, R. Y. Tsien, *J. Biol. Chem.* **1985**, *260*, 3440–3450.
[25] K. Suzuki, K. Tohda, Y. Tanda, H. Ohzora, S. Nishihama, H. Inoue, T. Shirai, *Anal. Chem.* **1989**, *61*, 382–384.
[26] V. C. Costa, F. A. C. Amorim, D. V. de Babos, E. R. Pereira-Filho, *Food Chem.* **2019**, *273*, 91–98.
[27] N. Ozbek, H. Tinas, A. E. Atespare, *Microchem. J.* **2019**, *144*, 474–478.
[28] D. Pan, J. Zhang, Z. Li, M. Wu, *Adv. Mater.* **2010**, *22*, 734–738.
[29] D. C. Marcano, D. V. Kosynkin, J. M. Berlin, A. Sinitskii, Z. Sun, A. Slesarev, L. B. Alemany, W. Lu, J. M. Tour, *ACS Nano* **2010**, *4*, 4806–4814.
[30] C.-M. Chen, J.-Q. Huang, Q. Zhang, W.-Z. Gong, Q.-H. Yang, M.-Z. Wang, Y.-G. Yang, *Carbon* **2012**, *50*, 659–667.
[31] a) T. Bala, B. L. V. Prasad, M. Sastry, M. U. Kahaly, U. V. Waghmare, *J. Phys. Chem. A* **2007**, *111*, 6183–6190; b) F. Ancillotti, G. Boschi, G. Perego, A. Zazzetta, *J. Chem. Soc., Dalton Trans.* **1977**, 901–905.
[32] R. Choudhary, S. Koppala, S. Swamiappan, *Journal of Asian Ceramic Societies* **2015**, *3*, 173–177.
[33] S. Kim, S. W. Hwang, M. K. Kim, D. Y. Shin, D. H. Shin, C. O. Kim, S. B. Yang, J. H. Park, E. Hwang, S. H. Choi, G. Ko, S. Sim, C. Sone, H. J. Choi, S. Bae, B. H. Hong, *ACS Nano* **2012**, *6*, 8203–8208.

Submitted: May 22, 2019
Accepted: July 18, 2019